*Acta Oceanol. Sin.*, 2020, Vol. 39, No. 7, P. 50–60
https://doi.org/10.1007/s13131-020-1623-z
http://www.hyxb.org.cn
E-mail: hyxbe@263.net

# Eastern equatorial Pacific SST seasonal cycle in global climate models: from CMIP5 to CMIP6

Zhenya Song[1, 2], Hailong Liu[3], Xingrong Chen[4]*

[1] First Institute of Oceanography, Ministry of Natural Resources, Qingdao 266061, China

[2] Laboratory for Regional Oceanography and Numerical Modeling, Pilot National Laboratory for Marine Science and Technology (Qingdao), Qingdao 266237, China

[3] School of Oceanography, Shanghai Jiaotong University, Shanghai 200240, China

[4] National Marine Environmental Forecasting Center, Ministry of Natural Resources, Beijing 100081, China

Received 15 August 2019; accepted 27 September 2019



**Abstract**

The sea surface temperature (SST) seasonal cycle in the eastern equatorial Pacific (EEP) plays an important role in the El Niño–Southern Oscillation (ENSO) phenomenon. However, the reasonable simulation of SST seasonal cycle in the EEP is still a challenge for climate models. In this paper, we evaluated the performance of 17 CMIP6 climate models in simulating the seasonal cycle in the EEP and compared them with 43 CMIP5 climate models. In general, only CESM2 and SAM0-UNICON are able to successfully capture the annual mean SST characteristics, and the results showed that CMIP6 models have no fundamental improvement in the model annual mean bias. For the seasonal cycle, 14 out of 17 climate models are able to represent the major characteristics of the observed SST annual evolution. In spring, 12 models capture the 1–2 months leading the eastern equatorial Pacific region 1 (EP1; 5°S–5°N, 110°–85°W) against the eastern equatorial Pacific region 2 (EP2; 5°S–5°N, 140°–110°W). In autumn, only two models, GISS-E2-G and SAM0-UNICON, correctly show that the EP1 and EP2 SSTs vary in phase. For the CMIP6 MME SST simulation in EP1, both the cold bias along the equator in the warm phase and the warm bias in the cold phase lead to a weaker annual SST cycle in the CGCMs, which is similar to the CMIP5 results. However, both the seasonal cold bias and warm bias are considerably decreased for CMIP6, which leads the annual SST cycle to more closely reflect the observation. For the CMIP6 MME SST simulation in EP2, the amplitude is similar to the observed value due to the quasi-constant cold bias throughout the year, although the cold bias is clearly improved after August compared with CMIP5 models. Overall, although SAM0-UNICON successfully captured the seasonal cycle characteristics in the EEP and the improvement from CMIP5 to CMIP6 in simulating EEP SST is clear, the fundamental climate models simulated biases still exist.

**Key words:** CMIP5, CMIP6, eastern equatorial Pacific, SST seasonal cycle

**Citation:** Song Zhenya, Liu Hailong, Chen Xingrong. 2020. Eastern equatorial Pacific SST seasonal cycle in global climate models: from CMIP5 to CMIP6. Acta Oceanologica Sinica, 39(7): 50–60, doi: 10.1007/s13131-020-1623-z

## 1 Introduction

The sea surface temperature (SST) seasonal cycle in the eastern equatorial Pacific (EEP) plays an important role in the El Niño–Southern Oscillation (ENSO) phenomenon, especially in the phase-locking of ENSO (Neelin et al., 2000). Although the sun crosses the equator twice a year, SST seasonal variation in the EEP exhibits a strong seasonal cycle with a March–April warm phase and an August–October cold phase (Mitchell and Wallace, 1992; Nigam and Chao, 1996), which is different from the semi-annual cycle in the western equatorial Pacific. There are numerous studies on understanding the mechanisms of the SST seasonal cycle (Mitchell and Wallace, 1992; Giese and Carton, 1994; Xie, 1994, 2004; Mechoso et al., 1995; Nigam and Chao, 1996; Dewitt and Schneider, 1999) and several dominant physical processes have been hypothesized to explain the seasonal cycle in the EEP (Xie, 2004), such as wind–evaporation–SST feedback, stratus–SST feedback and upwelling–SST feedback. Because the SST seasonal cycle in the EEP involves complex dynamical and physical interactions among climate subsystems, it usually serves as an indicator for the performance of global climate models.

Since the pioneering work of developing a climate model by Manabe and Bryan (1969), climate models have achieved significant progress and can provide credible basic climate simulation, particularly through the Coupled Model Intercomparison Project (CMIP). However, model biases still persist in the state-of-the-art climate models in terms of simulating the SST seasonal cycle in the EEP (Mechoso et al., 1995; Covey et al., 2000; Latif et al., 2001; Xie et al., 2007). De Szoeke and Xie (2008) compared the SST results of 14 global climate models in the CMIP phase 3 (CMIP3) and showed that eight out of these models had a robust

Foundation item: The National Key R&D Program of China under contract No. 2016YFA0602200; the Basic Scientific Fund for National Public Research Institute of China under contract No. 2016S03; the grant of Qingdao National Laboratory for Marine Science and Technology under contract Nos 2017ASTCP-ES04 and QNLM20160RP0101; the National Natural Science Foundation of China under contract No. 41776019; the Shanghai Natural Science Foundation under contract No. 16ZR1416200; the China-Korea Cooperation Project on Northwestern Pacific Climate Change and its Prediction.
*Corresponding author, E-mail: luckychen@nmefc.cn

**Table 1.** List of CMIP5 and CMIP6 global climate models with the name of the modeling center (or group) used in this study [1)]

| No. | Modeling center | CMIP5+ | | | | | CMIP6++ | | | | |
|---|---|---|---|---|---|---|---|---|---|---|---|
| | | Model name | CORR | | STD/°C | | Model name | CORR | | STD/°C | |
| | | | EP1 | EP2 | EP1 | EP2 | | EP1 | EP2 | EP1 | EP2 |
| 1 | BCC (China) | BCC-CSM1-1 (a) | 0.818 | 0.757 | 0.972 | 0.581 | BCC-CSM2-MR (a) | 0.828 | 0.578 | 1.075 | 0.461 |
| | | BCC-CSM1-1-m (b) | 0.866 | 0.731 | 1.208 | 1.088 | BCC-ESM1 (b) | 0.759 | 0.741 | 0.963 | 0.632 |
| 2 | BNU (China) | BNU-ESM | 0.888 | 0.832 | 1.290 | 0.966 | – | – | – | – | – |
| 3 | CAMS (China) | – | – | – | – | – | CAMS-CSM1-0 | 0.737 | 0.444 | 1.321 | 0.636 |
| 4 | CCCMA (Canada) | CanESM2 | 0.872 | 0.830 | 0.772 | 0.759 | CanESM5 | 0.546 | 0.755 | 0.953 | 0.569 |
| 5 | CCSR (Japan) | MIROC5 | 0.870 | 0.927 | 0.850 | 0.866 | MIROC6 | 0.992 | 0.955 | 0.928 | 1.063 |
| 6 | CMCC (Italy) | CMCC-CESM (a) | 0.938 | 0.845 | 1.140 | 0.680 | – | – | – | – | – |
| | | CMCC-CM (b) | 0.933 | 0.976 | 0.807 | 0.658 | – | – | – | – | – |
| | | CMCC-CMS (c) | 0.948 | 0.948 | 0.890 | 0.793 | – | – | – | – | – |
| 7 | CSRIO-BOM (Australia) | ACCESS1-0 (a) | 0.925 | 0.968 | 0.999 | 0.724 | – | – | – | – | – |
| | | ACCESS1-3 (b) | 0.650 | 0.515 | 0.852 | 0.362 | – | – | – | – | – |
| 8 | CSRIO-QCCCE (Australia) | CSIRO-Mk3-6-0 | 0.844 | 0.955 | 1.120 | 0.966 | – | – | – | – | – |
| 9 | EC-Earth (Europe) | – | – | – | – | – | EC-Earth3 (a) | 0.910 | 0.908 | 1.219 | 0.626 |
| | | | | | | | EC-Earth3-Veg (b) | 0.888 | 0.890 | 1.301 | 0.668 |
| 10 | FIO (China) | FIO-ESM | 0.912 | 0.761 | 0.778 | 0.702 | – | – | – | – | – |
| 11 | GFDL (USA) | GFDL-CM2p1 (a) | 0.869 | 0.829 | 1.371 | 1.054 | GFDL-CM4 | 0.895 | 0.900 | 1.279 | 0.989 |
| | | GFDL-CM3 (b) | 0.650 | 0.373 | 1.127 | 0.539 | – | – | – | – | – |
| | | GFDL-ESM2G (c) | 0.887 | 0.898 | 1.645 | 0.989 | – | – | – | – | – |
| | | GFDL-ESM2M (d) | 0.818 | 0.694 | 1.223 | 0.753 | – | – | – | – | – |
| 12 | Hadley Center (UK) | HadCM3 (a) | 0.843 | 0.935 | 0.623 | 0.751 | HadGEM3-GC31-LL | 0.826 | 0.816 | 1.442 | 0.884 |
| | | HadGEM2-A0 (b) | 0.942 | 0.789 | 1.250 | 0.759 | – | – | – | – | – |
| | | HadGEM2-CC (c) | 0.879 | 0.780 | 1.184 | 0.770 | – | – | – | – | – |
| | | HadGEM2-ES (d) | 0.938 | 0.863 | 1.217 | 0.834 | – | – | – | – | – |
| 13 | INM (Russia) | INM-CM4 | 0.488 | 0.333 | 0.980 | 1.006 | – | – | – | – | – |
| 14 | IPSL (France) | IPSL-CM5A-LR (a) | 0.499 | 0.589 | 1.179 | 0.776 | IPSL-CM6A-LR | 0.879 | 0.977 | 1.260 | 1.209 |
| | | IPSL-CM5A-MR (b) | 0.581 | 0.517 | 1.290 | 0.704 | – | – | – | – | – |
| | | IPSL-CM5B-LR (c) | 0.543 | 0.200 | 0.711 | 0.488 | – | – | – | – | – |
| 15 | LASG (China) | FGOALS-g2 (a) | 0.945 | 0.911 | 0.788 | 0.889 | – | – | – | – | – |
| | | FGOALS-s2 (b) | 0.918 | 0.976 | 0.716 | 1.230 | | | | | |
| 16 | Met Office (UK) | – | – | – | – | – | UKESM1-0-LL | 0.839 | 0.844 | 1.456 | 0.861 |
| 17 | Météo-France (France) | CNRM-CM5 | 0.944 | 0.911 | 1.161 | 1.197 | CNRM-CM6 (a) | 0.821 | 0.944 | 1.416 | 1.145 |
| | | | | | | | CNRM-ESM2 (b) | 0.844 | 0.938 | 1.584 | 1.375 |
| 18 | MPI (Germany) | MPI-ESM-LR (a) | 0.944 | 0.924 | 0.897 | 0.885 | – | – | – | – | – |
| | | MPI-ESM-MR (b) | 0.931 | 0.959 | 0.893 | 0.844 | – | – | – | – | – |
| | | MPI-ESM-P (c) | 0.910 | 0.877 | 0.834 | 0.842 | – | – | – | – | – |
| 19 | MRI (Japan) | MRI-CGCM3 (a) | 0.625 | 0.231 | 1.139 | 0.592 | – | – | – | – | – |
| | | MRI-ESM1 (b) | 0.587 | 0.215 | 1.109 | 0.576 | – | – | – | – | – |
| 20 | NASA (USA) | GISS-E2-H (a) | 0.825 | 0.785 | 0.734 | 0.491 | GISS-E2-G (a) | 0.830 | 0.598 | 0.963 | 0.707 |
| | | GISS-E2-R (b) | 0.927 | 0.876 | 0.828 | 0.610 | GISS-E2-H (b) | 0.870 | 0.733 | 0.801 | 0.657 |
| | | GISS-E2-R-CC (c) | 0.927 | 0.878 | 0.808 | 0.610 | | | | | |
| 21 | NCAR (USA) | CCSM4 (a) | 0.881 | 0.781 | 0.862 | 0.704 | CESM2 | 0.949 | 0.917 | 1.353 | 0.989 |
| | | CESM1-BGC (b) | 0.880 | 0.720 | 0.944 | 0.668 | – | – | – | – | – |
| | | CESM1-CAM5 (c) | 0.974 | 0.930 | 1.472 | 1.159 | – | – | – | – | – |
| | | CESM1-CAM5-1-FV2 (d) | 0.907 | 0.803 | 1.107 | 0.778 | – | – | – | – | – |
| | | CESM1-FASTCHEM (e) | 0.883 | 0.763 | 0.871 | 0.692 | – | – | – | – | – |
| | | CESM1-WACCM (f) | 0.937 | 0.896 | 1.050 | 0.761 | – | – | – | – | – |
| 22 | NCC (Norway) | NorESM1-M (a) | 0.722 | 0.639 | 0.664 | 0.496 | – | – | – | – | – |
| | | NorESM1-ME (b) | 0.724 | 0.837 | 0.796 | 0.631 | – | – | – | – | – |
| 23 | SNU (South Korea) | – | – | – | – | – | SAM0-UNICON | 0.989 | 0.903 | 1.182 | 0.744 |
| | Multi-model ensemble mean | – | 0.895 | 0.888 | 0.935 | 0.684 | – | 0.883 | 0.916 | 1.159 | 0.771 |
| | ERSST v4 | – | 1 | 1 | 1.428 | 0.865 | – | 1 | 1 | 1.428 | 0.865 |

Note: [1)]The correlation coefficient between model and observation (CORR) and standard deviation of seasonal cycle (STD) are also reported. The "–" stands for model (or data) not available now. The blue number means improvement since CMIP5. + For all models, the first ensemble member of the historical experiment ("r1i1p1") was analyzed over the period 1949–2005. ++ For all models, the first ensemble member of the historical experiment ("r1i1p1f1") was analyzed over the period 1949–2005.

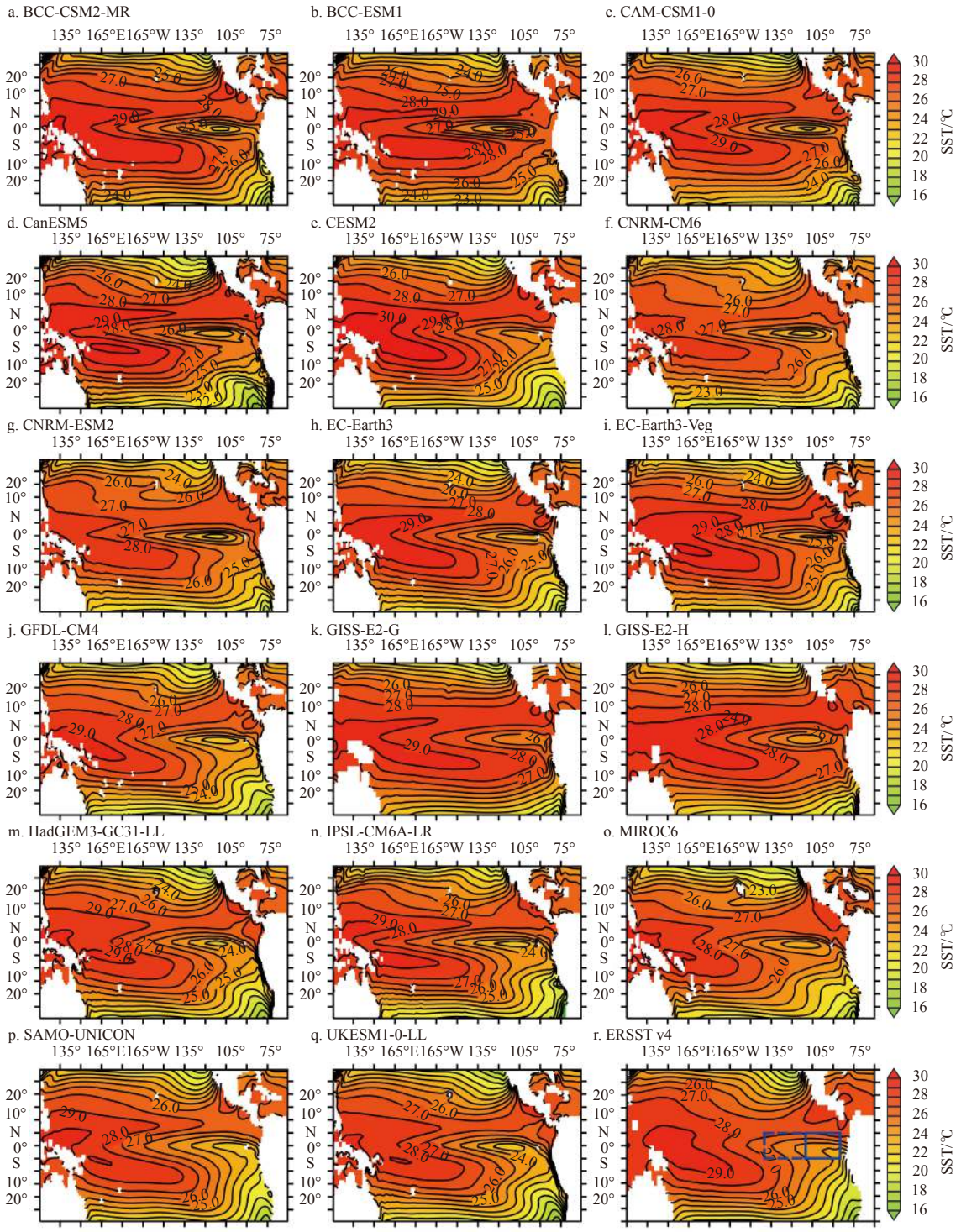


**Fig. 1.** Distributions of sea surface temperature (SST) climatology of 1949–2005 in the tropical Pacific. Blue solid and dashed boxes in ERSST v4 indicate the EP1 region and EP2 regions, respectively.

SST semiannual cycle in the EEP. Recently, Song et al. (2014) evaluated 18 global climate models in the CMIP phase 5 (CMIP5) and found that most of the models can capture the SST seasonal cycle signal and westward propagation character in the EEP but with weaker amplitude compared to observation. The model outputs of the CMIP phase 6 (CMIP6) were released recently and include the latest version of models participating in CMIP5 and several new models. Therefore, a natural question is how well the SST seasonal cycle in the EEP is reproduced in CMIP6 models.

This study aims to use the outputs of the CMIP6 historical simulations to evaluate the EEP SST seasonal cycle simulation in the latest versions of climate models. A brief description of the models and validation datasets used in this study are presented in Section 2. Section 3 compares the simulations results between

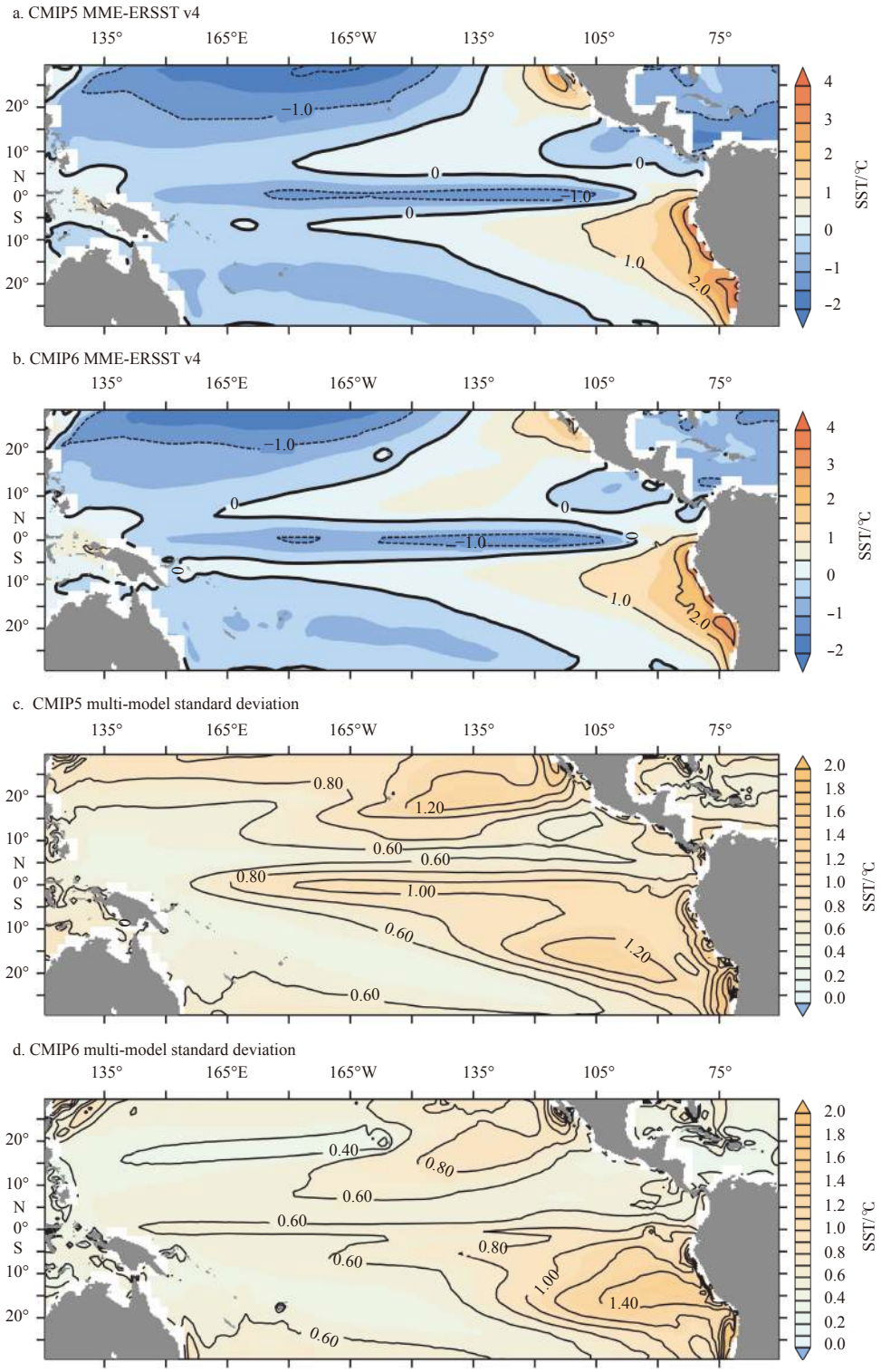


**Fig. 2.** Sea surface temperature (SST) biases of CMIP5 multi-model ensemble mean (MME) (a), CMIP6 MME relative to ERSST v4 (b), and multi-model standard deviation of CMIP5 (c), CMIP6 (d) in the tropical Pacific.

CMIP5 and CMIP6 models, and Section 4 provides the discussion and conclusion.

## 2 Data and methodology

The first realization of the historical simulations from 43 CMIP5 (r1i1p1) and 17 CMIP6 (r1i1p1f1) climate models used are summarized in Table 1. Each historical simulation was integrated from a pre-industry spin-up experiment and was then forced by solar, volcanic, aerosol, and greenhouse gas forcing for the period of 1850–2005 for CMIP5 historical experiments (Taylor et al., 2012) and 1850–2014 for CMIP6 historical experiments (Eyring et al., 2016). In this study, we select the monthly outputs

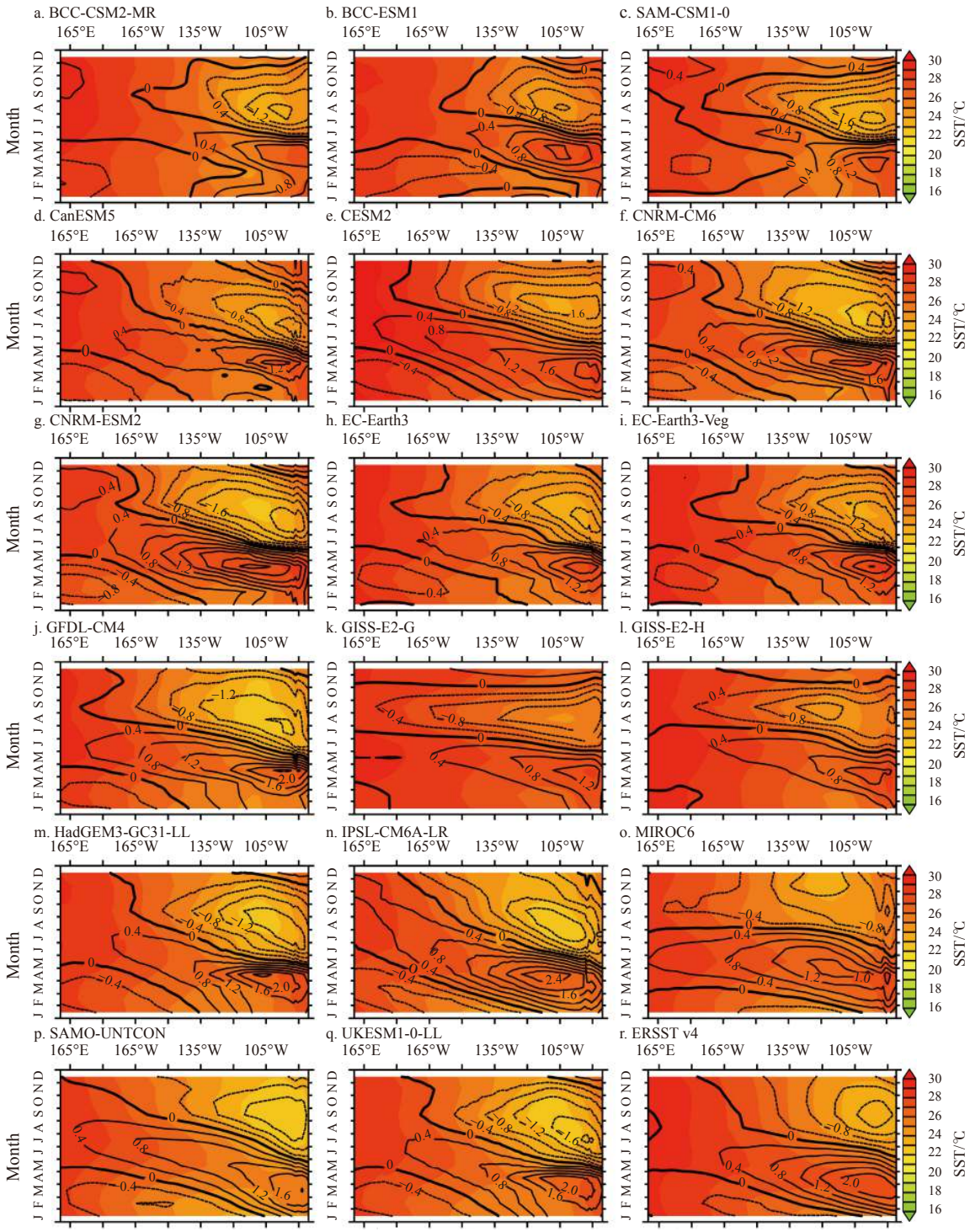


**Fig. 3.** Seasonal cycle of sea surface temperature (SST) in the eastern equatorial Pacific (EEP). Shading represents climatological SST and contours represent SST anomalies relative to the climatological annual mean.

from 1949 to 2005 for analysis.

Simulation results were compared with the National Oceanic and Atmospheric Administration extended reconstructed SST version 4 (ERSST v4) (Huang et al., 2016). This dataset is a global monthly gridded dataset generated by using *in situ* data from the International Comprehensive Ocean-Atmosphere Dataset (ICOADs) with missing data filled in by statistical methods. To validate model simulations, we used the ERSST monthly data from 1949 to 2005. The model simulation and observation data are interpolated to a 1° × 1° grid.

As suggested by Song et al. (2014), two regions with different features in the EEP are selected for analysis in this study. The first is the region from 5°S to 5°N, 110° to 85°W (hereafter called "EP1"; Fig. 1r blue solid box), which has the large amplitude of the SST seasonal cycle. Another is the transition region (5°S–5°N, 140°–110°W) (hereafter called "EP2"; Fig. 1r blue dash box) with a

weaker seasonal cycle and one-month lag with EP1 in the warm phase.

## 3 Results

### 3.1 *Annual mean*

The mean state, such as the annual mean SST, is important in influencing the characteristics of natural variability. It is necessary to first examine the patterns of the annual mean SST of the EEP shown in Fig. 1. The observed SST (ERSST v4, Fig. 1r) reaches 29°C in the western warm pool region, and along the equator the SST decreases to 27°C with strong meridional gradients in the eastern Pacific. Compared with the observations, only CESM2 (Fig. 1e) and SAM0-UNICON (Fig. 1p) are able to capture its character. The other models exhibit a uniform minimum center of SST in the EEP, which dramatically increases the SST gradient to the south of equator in those models. Overall the SST range in the models at the equator is comparable to the range of observations.

The difference between the multi-model ensemble mean and observation shows the model bias of CMIP5 (Fig. 2a) and CMIP6 (Fig. 2b). Whether in terms of spatial pattern or values, the biases of two generations of climate models are quite similar. A cold bias extends from the west equatorial pacific to 90°W. For CMIP6 models, the region with cold bias less than –1°C is smaller; however, the cold bias tends to be stronger compared with CMIP5 models. Compared with the values of multi-model standard deviation of CMIP5 (Fig. 2c) and CMIP6 (Fig. 2d), which can be regarded as the proxy for intermodal difference (Jang et al., 2011), there is no distinguishable difference for the warm bias along the coasts of Mexico and Peru and the cold bias along the coast of Central America between the CMIP5 and CMIP6 models. This indicates that CMIP6 models have no fundamental improvement in model mean bias.

### 3.2 *Seasonal cycle*

As discussed in Song et al. (2014) and shown in Fig. 3r (ERSST v4), the observed EEP SST reaches a peak at 27°C in March and April and reaches a minimum of 23°C in September and October. This seasonal cycle is pronounced primarily in the region between 110 and 85°W along the equator (EP1). And there is almost no seasonal cycle to the west of 140°W (EP1), where SST shows a much weaker seasonal cycle compared with EP1. The conclusion from Song et al. (2014) holds true based on ERSST v4. The warming in EP1 tends to propagate westward and takes a 1-month lead over EP2 in the warm phase. After June, the variations in EP1 and EP2 are in phase. This indicates that the mechanisms controlling the warm and cold phases in the EEP vary with season. Next, we focus on the two regions to evaluate the CMIP6 models.

Fourteen models, shown in Fig. 3, are able to represent the major characteristics of the observed SST seasonal cycle and are classified as Group 1, which includes BCC-CSM2-MR (Fig. 3a), BCC-ESM1 (Fig. 3b), CAM-CSM1-0 (Fig. 3c), CanESM5 (Fig. 3d), CESM2 (Fig. 3e), CNRM-CM6 (Fig. 3f), CNRM-ESM2 (Fig. 3g), EC-Earth3 (Fig. 3h), EC-Earth3-Veg (Fig. 3i), GFDL-CM4 (Fig. 3j), HadGEM3-GC31-LL (Fig. 3m), IPSL-CM6A-LR (Fig. 3n), SAM0-UNICON (Fig. 3p), and UKESM1-0-LL (Fig. 3q). The remaining three models, GISS-E2-G (Fig. 3k), GISS-E2-H (Fig. 3l) and MIROC6 (Fig. 3o), are classified as group 2 which are not able to reproduce the westward propagation of the EP1 warming. The ensemble mean of the CMIP6 models replicates the observed patterns and warm/cold season values more realistically than CMIP5 models (Fig. 4). The warm/cold anomaly center in CMIP6 reaches +1.99/–1.63°C, respectively, close to the observed +2.39/–1.80°C. CMIP5 models are also able to capture the annual SST evolution pattern, but the warm/cold anomaly center barely reaches +1.62/–1.39°C. Thus, it shows a slight improvement at this point.

Furthermore, the regional averaged SSTs over EP1 and EP2 are shown in Fig. 5. Based on the observed ERSST, the EP2 SST follows the variation of EP1 in March and April with a 1–2 month lag. In the following seasons, EP2 SST varies in phase with EP1 when the Pacific cold tongue develops. In spring, 12 models, including BCC-CSM2-MR (Fig. 5a), BCC-ESM1 (Fig. 5b), CAM-CSM1-0 (Fig. 5c), CanESM5 (Fig. 5d), CNRM-CM6 (Fig. 5f), EC-Earth3 (Fig. 5h), EC-Earth3-Veg (Fig. 5i), GISS-E2-G (Fig. 5k), GISS-E2H (Fig. 5l), IPSL-CM6A-LR (Fig. 5n), MIROC6 (Fig. 5o), and SAM0-UNICON (Fig. 5p), capture the 1-2 month lead of EP1 against EP2. In autumn, only two models, GISS-E2-G (Fig. 5k) and SAM0-UNICON (Fig. 5p), show that the EP1 and EP2 SSTs vary in phase. It is notable that the SAM0-UNICON model demonstrates high performance in simulating the EEP SST.

The SST amplitude of CMIP6 MME in EP1 increases to 3.2°C from 2.7°C of CMIP5 MME (Fig. 6). Compared with the observed amplitude of 3.8°C, CMIP6 MME makes progress in improving the cold bias in the boreal spring and the warm bias in the boreal autumn. However, for the CMIP6 MME in EP2, it seems that the cold bias from August to December is stronger than CMIP5 and thus the amplitude of is slightly larger than the amplitude of CMIP5 MME. Overall, the EP2 SST amplitudes of both CMIP6 and CMIP5 MME are comparable to the observation with a quasi-constant cold bias throughout the year. It is also clear that the EP2 peak of CMIP6 MME correctly occurs in March while the EP1 peak is also in March. Therefore, the lag relationship between EP1 and EP2 is misrepresented.

Figures 7a and c and Figs 7b and d show that the SST bias pat-

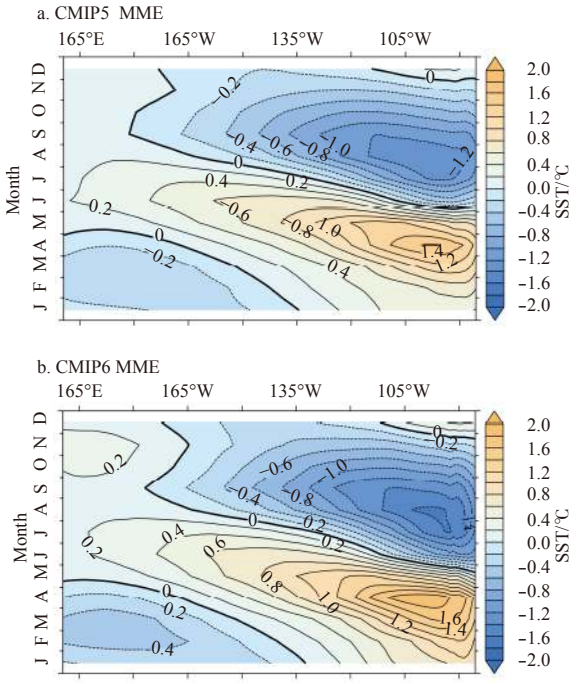


**Fig. 4.** Seasonal cycle of sea surface temperature (SST) of (a) CMIP5 multi-model ensemble mean (MME) and (b) CMIP6 MME in the eastern equatorial Pacific.

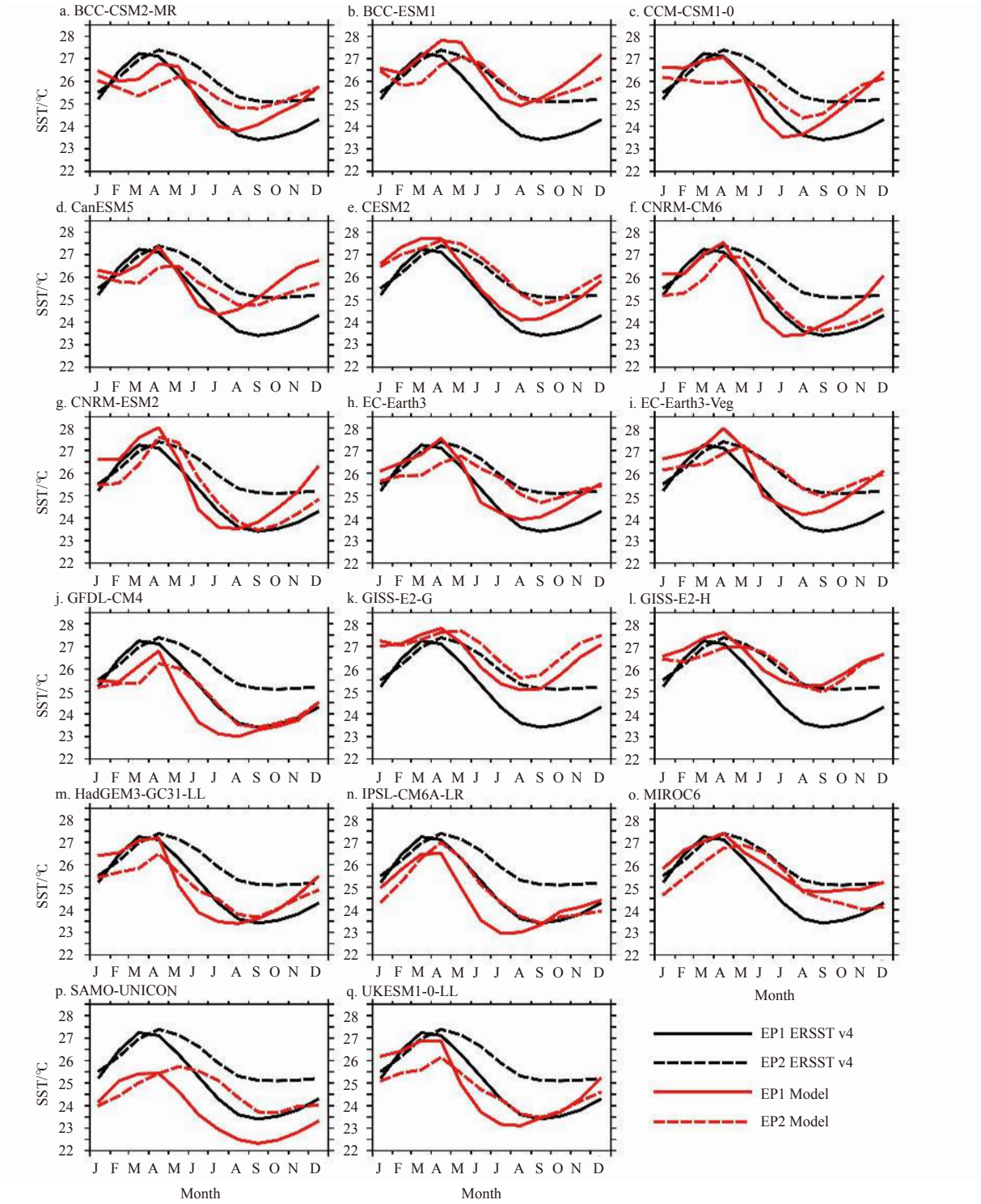


**Fig. 5.** Sea surface temperature (SST) seasonal cycle for eastern equatorial Pacific (EEP) region 1 (EP1; 5°S–5°N, 110°–85°W; solid line) and EEP region 2 (EP2; 5°S–5°N, 140°–110°W; dashed line). The black curves are the ERSST, and the red lines are model outputs.

tern is consistent between CMIP5 and CMIP6 models and between spring and autumn, respectively. The difference between CMIP5 and CMIP6 models (Figs 7e, f) further shows that in April there is no significant improvement in the simulated bias except in the coastal region from Mexico to Peru. The coastal warm bias and cold bias decrease simultaneously. In August, the CMIP6 warm bias in the southeastern Pacific is considerably improved, which corresponds to the improvement in EP1 and EP2 averaged SST after July in Fig. 6. Though we can see the improvement of the CMIP6 SST simulation, the mechanism dominating the bias still holds true (Song et al., 2014) such that in EP1, the warm SST bias develops in August and expands from the southeastern Pacific associated with a southward wind bias. This wind bias reduces the southeastern trade wind over EP1 and leads to weaker latent heat loss from the ocean and thus leads to a warm SST bias.

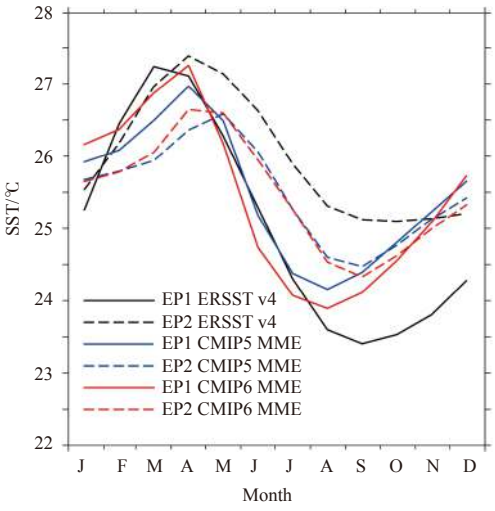


**Fig. 6.** Multi-model ensemble mean (MME) sea surface temperature (SST) for the eastern equatorial Pacific (EEP) region 1 (EP1; 5°S–5°N, 110°–85°W; solid line) and EEP region 2 (EP2; 5°S–5°N, 140°–110°W; dashed line) seasonal cycle. Black, blue and red lines represent ERSST, CMIP5 MME and CMIP6 MME, respectively.

A detailed model to model comparison from the same institution is summarized in Fig. 8. For the EP1 simulation, the CMIP6 models from BCC, CCCMA, Hadley Center, and Meteo-France actually have less correlation with observations compared with CMIP5 models. The increase in correlation from CMIP5 to CMIP6 of GFDL, IPSL, and NCAR indicates model improvement. CCCMA and SNU are the models with the highest correlation with observations. From the view of the ensemble mean, the CMIP5 and CMIP6 MME (Fig. 8a) have no significant differences, although the CMIP6 spread is narrower and its standard deviation is closer to that of observations (Fig. 8b). For the EP2 simulation, the CMIP5 models from modeling centers 1 (BCC), 4 (CCCMA), 12 (Hadley Center), and 20 (NASA) have better performance. The CMIP6 models from modeling centers 5 (CCSR), 11 (GFDL), 14 (IPSL), 17 (Météo-France), and 21 (NCAR) show clear improvement. The ensemble mean of CMIP6 demonstrates higher correlation and less spread (Fig. 8c) and is closer to observations in terms of standard deviation (Fig. 8d), all of which corresponds to model improvement.

## 4 Discussion and summary

We comprehensively evaluated the performance of CMIP6 CGCMs in simulating the seasonal cycle in the EEP and compared them with the last generation of models. Compared with

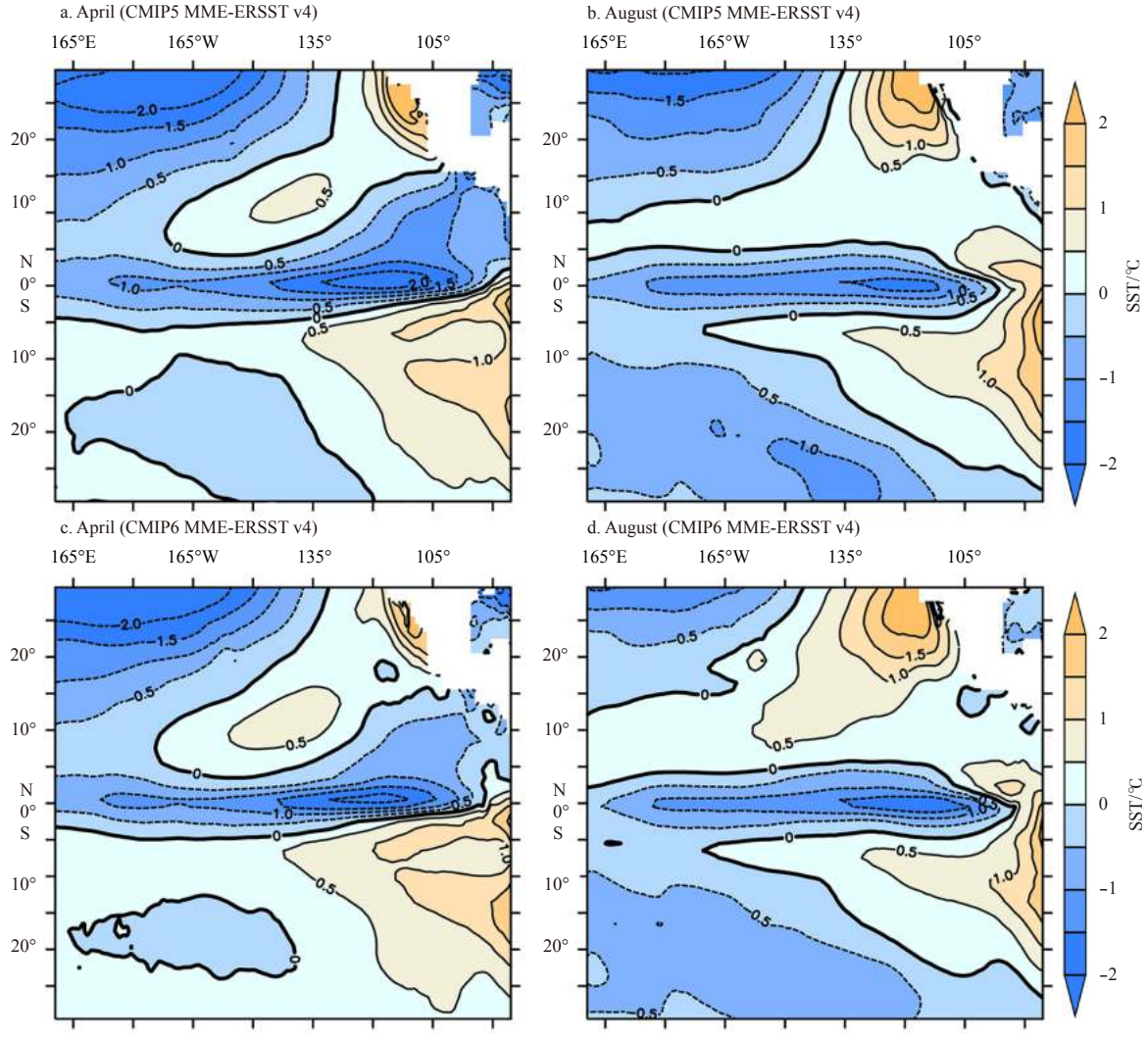


**Fig. 7.**

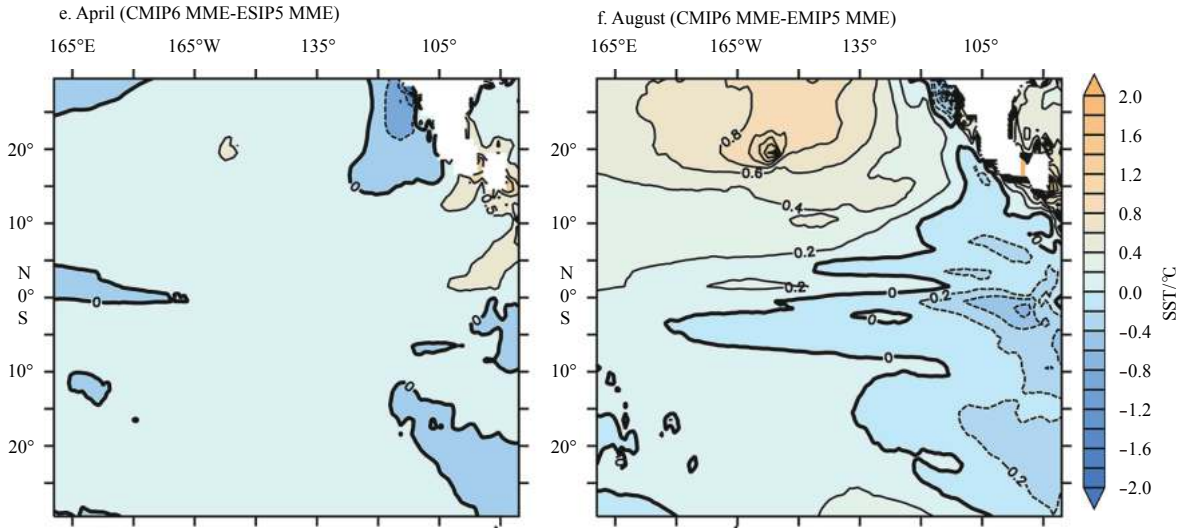


**Fig. 7.** Multi-model ensemble mean (MME) SST simulated biased in CMIP5 MME (a) and CMIP6 MME (c) in April; CMIP5 MME (b) and CMIP5 MME (d) in August. Figures e and f represent the differences between CMIP6 and CMIP5 MME in April and August, respectively.

observations, only CESM2 and SAM0-UNICON are able to successfully capture the annual mean SST characters. There is no obvious difference for the warm bias along the coasts of Mexico and Peru and the cold bias along the coast of Central America between the CMIP5 and CMIP6 models. This indicates that CMIP6 models have no fundamental improvement in model annual mean bias.

For the seasonal cycle, 14 models out of a total of 17 models are able to represent the major characteristics of the observed SST annual evolution. In spring, 12 models capture the 1–2

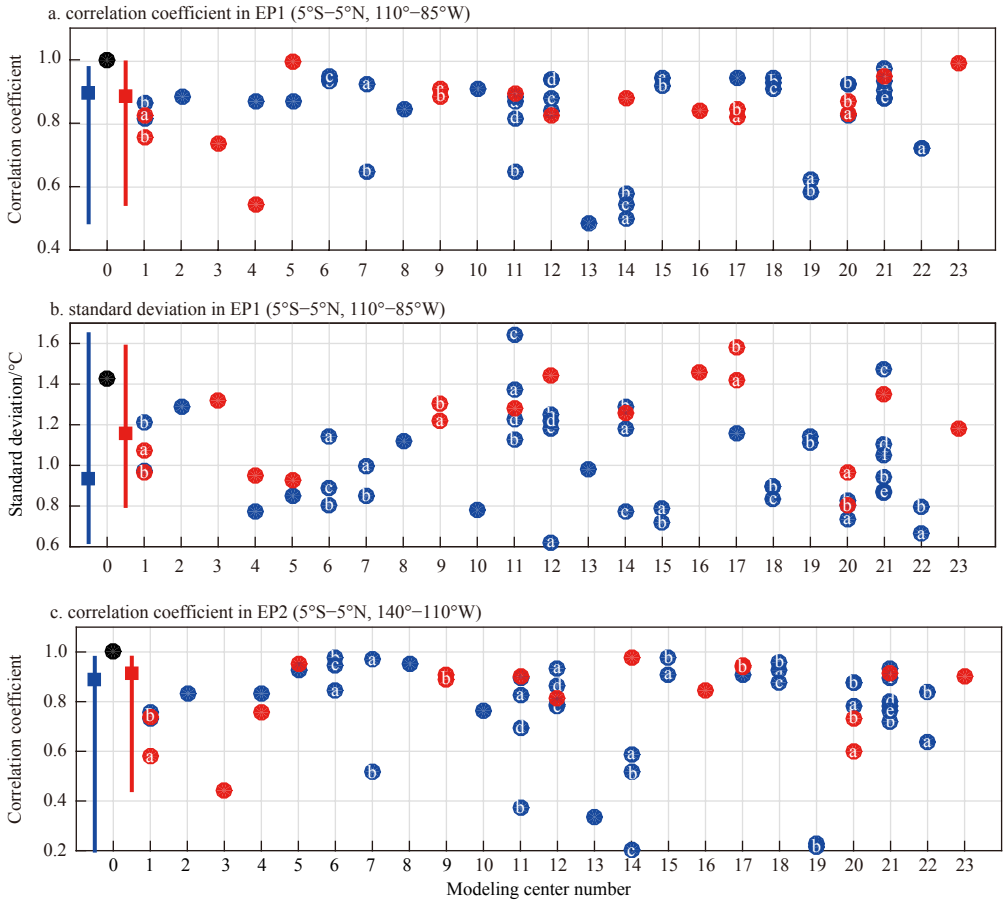


**Fig. 8.**

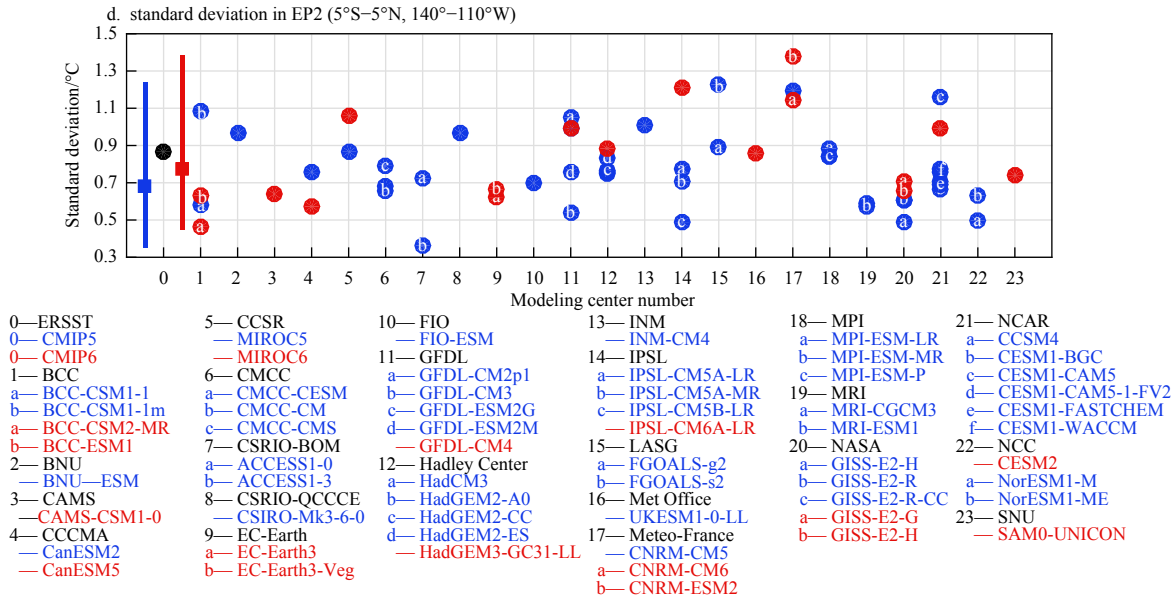


**Fig. 8.** Sea surface temperature (SST) seasonal cycle metrics for CMIP5 (blue) and CMIP6 (red) climate models. a and c. Correlation coefficient of the SST seasonal cycle in eastern equatorial Pacific (EEP) region 1 (EP1; 5°S–5°N, 110°–85°W) and region 2 (EP2; 5°S–5°N, 140°–110°W); b and d. the standard deviations of SST seasonal cycle in EP1 and EP2 (°C). ERSST are shown as black solid circles. The CMIP5 and CMIP6 multi-model ensemble means are shown as squares on the left of each panel with the whiskers representing the inter-model spread.

month lead of EP1 against EP2. In autumn, only two models, GISS-E2-G and SAM0-UNICON, correctly show that the EP1 and EP2 SSTs vary in phase. Similar to the CMIP5 models, for the CMIP6 MME SST simulation in EP1, both the cold bias along the equator in the warm phase and the warm bias in the cold phase lead to a weaker annual SST cycle in the CGCMs. However, both the seasonal cold bias and warm bias are considerably decreased for CMIP6 and lead the annual SST cycle being closer to the observations. For the CMIP6 MME SST simulation in EP2, the amplitude is similar to the observations due to the quasi-constant cold bias throughout the year. Overall, the improvement from CMIP5 to CMIP6 in simulating EEP SST is clear, but the fundamental CGCMs bias still exists.

***Acknowledgements***

We acknowledge two anonymous reviewers for their constructive comments and recommendations on ways of improving the manuscript. We thank all the modeling groups, the PCMDI and the World Climate Research Programme's Working Group on Coupled Modeling for their efforts in making available the CMIP multi-model datasets.

**References**

Covey C, Abe-Ouchi A, Boer G J, et al. 2000. The seasonal cycle in coupled ocean-atmosphere general circulation models. Climate Dynamics, 16(10–11): 775–787, doi: 10.1007/s003820000081

De Szoeke S P, Xie Shangping. 2008. The tropical eastern Pacific seasonal cycle: Assessment of errors and mechanisms in IPCC AR4 coupled ocean-atmosphere general circulation models. Journal of Climate, 21(11): 2573–2590, doi: 10.1175/2007JCLI1975.1

DeWitt D G, Schneider E K. 1999. The processes determining the Annual Cycle of Equatorial Sea surface temperature: a coupled general circulation model perspective. Monthly Weather Review, 127(3): 381–395, doi: 10.1175/1520-0493(1999)127<0381:TPDTAC>2.0.CO;2

Eyring V, Bony S, Meehl G A, et al. 2016. Overview of the Coupled Model Intercomparison Project Phase 6 (CMIP6) experimental design and organization. Geoscientific Model Development, 9(5): 1937–1958, doi: 10.5194/gmd-9-1937-2016

Giese B S, Carton J A. 1994. The seasonal cycle in coupled ocean-atmosphere model. Journal of Climate, 7(8): 1208–1217, doi: 10.1175/1520-0442(1994)007<1208:TSCICO>2.0.CO;2

Huang Boyin, Thorne P W, Smith T M, et al. 2016. Further exploring and quantifying uncertainties for Extended Reconstructed Sea Surface Temperature (ERSST) Version 4 (v4). Journal of Climate, 29(9): 3119–3142, doi: 10.1175/JCLI-D-15-0430.1

Jang C J, Park J, Park T, et al. 2011. Response of the ocean mixed layer depth to global warming and its impact on primary production: a case for the North Pacific Ocean. ICES Journal of Marine Science, 68(6): 996–1007, doi: 10.1093/icesjms/fsr064

Latif M, Sperber K, Arblaster J, et al. 2001. ENSIP: the El Nino simulation intercomparison project. Climate Dynamics, 18(3/4): 255–276, doi: 10.1007/s003820100174

Manabe S, Bryan K. 1969. Climate calculations with a combined ocean-atmosphere model. Journal of the Atmospheric Sciences, 26(4): 786–789, doi: 10.1175/1520-0469(1969)026<0786:CCWACO>2.0.CO;2

Mechoso C R, Robertson A W, Barth N, et al. 1995. The seasonal cycle over the tropical Pacific in coupled ocean-atmosphere general circulation models. Monthly Weather Review, 123(9): 2825–2838, doi: 10.1175/1520-0493(1995)123<2825:TSCOTT>2.0.CO;2

Mitchell T P, Wallace J M. 1992. The annual cycle in equatorial convection and sea surface temperature. Journal of Climate, 5(10): 1140–1156, doi: 10.1175/1520-0442(1992)005<1140:TACIEC>2.0.CO;2

Neelin J D, Jin Feifei, Syu H H. 2000. Variations in ENSO phase locking. Journal of Climate, 13(14): 2570–2590, doi: 10.1175/1520-0442(2000)013<2570:VIEPL>2.0.CO;2

Nigam S, Chao Yi. 1996. Evolution dynamics of tropical ocean-atmosphere annual cycle variability. Journal of Climate, 9(12): 3187–3205, doi: 10.1175/1520-0442(1996)009<3187:EDOTOA>2.0.CO;2

Song Z Y, Liu H L, Wang C Z, et al. 2014. Evaluation of the eastern equatorial Pacific SST seasonal cycle in CMIP5 models. Ocean Science, 10(5): 837–843, doi: 10.5194/os-10-837-2014

Taylor K E, Stouffer R J, Meehl G A. 2012. An overview of CMIP5 and the experiment design. Bulletin of the American Meteorological Society, 93(4): 485–498, doi: 10.1175/BAMS-D-11-00094.1

Xie Shangping. 1994. On the genesis of the equatorial annual cycle. Journal of Climate, 7(12): 2008–2013, doi: 10.1175/1520-0442(1994)007<2008:OTGOTE>2.0.CO;2

Xie Shangping. 2004. The shape of continents, air-sea interaction, and the rising branch of the Hadley circulation. In: Diaz H F, Bradley R S, eds. The Hadley Circulation: Present, Past and Future. Dordrecht: Springer, 121–152, doi: 10.1007/978-1-4020-2944-8_5

Xie Shangping, Miyama T, Wang Yuqing, et al. 2007. A regional ocean-atmosphere model for eastern Pacific climate: toward reducing tropical biases. Journal of Climate, 20(8): 1504–1522, doi: 10.1175/JCLI4080.1